Upcoming damage size quantification in aeronautic composite structures based on imaging results post-processing

William Briand, Marc Rébillat, Mikhail Guskov and Nazih Mechbal

Abstract

In this paper, a damage quantification strategy relying on post-processing of Lamb wave based damage localization results is presented. This method is able to predict the upcoming sizes of a delamination after a training step. Inputs of the proposed method are localization index maps produced by damage localization algorithms and representing the presence likelihood of a damage over the structure under study. The area covered by a high localization index around the estimated damage location are then extracted from these spatial probability maps. A data-driven model representing the mathematical relationship between this quantification feature and the actual size of the damage is finally inferred and used to predict future damage size. The proposed method is successfully validated on experimental data coming from CFRP plate samples equipped with piezoelectric transducers. Delaminations induced by fatigue testing and laser shock are studied. The sensitivity of the method to input frequency and damage localization algorithms parameters is assessed and a method to automatically select its own parameters is proposed. Furthermore, it is demonstrated that a model can be confidently learned on a given CFRP plate sample and transferred to predict damage size on another similar CFRP plate sample.

Keywords

Structural health monitoring, damage imaging, damage quantification, composite aeronautic structures, Lamb wave, growth monitoring, supervised machine learning

1. Introduction

Maintenance represents a significant cost for airlines since structural integrity checks require to regularly ground aircrafts for several days (Ackert, 2010). These inspections are fixed interval with a rate provided by the airplane constructor. Nevertheless, as the current state of the structure is unknown, this rate is not condition-based and thus airplane are grounded whereas it is not needed most of the time. That is why real time monitoring of structures is of high interest in aeronautics. This research field is known as Structural Health Monitoring (SHM). Various techniques are used to monitor possible damage apparition in composite aeronautical structures. One of the most common is the emission and reception of ultrasonic Lamb waves (Giurgiutiu, 2007; Su and Ye, 2009). Such waves can propagate over long distances in large structures thanks to their small attenuation ratio. Moreover, Lamb waves are easy to generate at high frequencies (and thus short wavelengths) using ultrasonic transducers (such as piezoelectric elements). It makes them able to interact even with small damages (Ashwin et al., 2014; Shen and Cesnik, 2017; Worden et al., 2007). A common SHM system to generate and sense Lamb waves is a network of piezoelectric elements acting both as actuators and sensors bonded on the surface of the structure monitored (Giurgiutiu, 2005; Wang and Shen, 2019). Robust SHM algorithms based on Lamb waves have already shown great results for damage detection and localization purposes in composite structures (Su and Ye, 2009). However, there is still a huge need for reliable algorithms for damage quantification of such structures. This task is very challenging since

PIMM, Arts et Metiers Institute of Technology, CNRS, Cnam, HESAM University, Paris, France

Corresponding author:
William Briand, PIMM Laboratory, Arts et Mtiers, 151 Boulevard de l'Hpital, Paris 75013, France.
Email: william.briand@ensam.eu

the interaction between the incident wave and the delamination induced non-linearity, as noticed in Dafydd and Khodaei (2020). The experimental study focuses on three impacts with different energy level and it is demonstrated that the damage size has a high influence on the maximum of the envelope received signal. One existing method for damage quantification by means of Lamb waves consists in identifying and computing a relevant damage index that varies with the size of the damage (Liu et al., 2012). Another approach that has been proposed in the literature consists in training an Artificial Neural Network (ANN) on simulated data. The size of a damage is then estimated using experimental data processed by this ANN (Su and Ye, 2005). Statistical methods have also been investigated. Bayesian updating techniques have been applied to crack size (Yang et al., 2016) and delamination assessments (Peng et al., 2013). Multi-class classification for damage quantification with a support vector machine has been also been successfully validated on a beam (Ghrib et al., 2018).

In this paper, a damage quantification strategy based on post-processing of damage localization results is presented. Such a method allows for damage size assessment of a delaminated area by post-processing the images produced by any damage localization algorithm. Damage localization algorithms take raw signals from sensor as input and return a map of index. This index represents the likelihood of presence of a damage over the surface of the structure under study. From this spatial probability map, a region of high localization index is identified around the estimated damage location and the area of this region is computed. A data-driven model representing the mathematical relationship between this feature and the actual size of the damage is then inferred. The spatial probability maps provided by several damage localization algorithms have been investigated. Time of Arrival (ToA) (Fendzi et al., 2016) method is a multilateration technique used for localization. Its underlying idea is to compute the difference between the travel time of the wave on the direct path (actuator-sensor) and the travel time of the scattered signal on the secondary path (actuator-damage-sensor). The equations to be solved lead to a locus of possible damage positions under the form of an ellipse. Time difference of arrival (TDoA) (Fendzi et al., 2016) is based on the same principle. In this approach, difference of time of arrival of the wave scattered by the damage are computed at two sensors. This gives a hyperbola of possible positions. In the delay-and-sum method (DAS) (Michaels and Michaels, 2007; Qiu et al., 2013) for each point of the structure under interest and each actuator-sensor path, time of arrival of the Lamb waves is computed as if there was a damage at this position. Then the residual of the signal is computed (i.e. the difference of magnitude between the reference signal and the one that is tested). RAPID (Reconstruction Algorithm for the Probabilistic Inspection of Damage) (Sharif-Khodaei and Aliabadi, 2014; Zhao et al., 2007) algorithm consists in computing the probability of a defect occurrence using the relative amplitude of the signal change on each actuator-sensor path. This probability is computed using the signal difference coefficient and a ratio representing how far is the point from the direct path.

Some attempts have already been carried out to post-process Lamb wave based damage localization results for damage size quantification purposes. An algorithm based on ToA localization has been developed by Sorrentino and De Fenza to assess the size of an impact. Each tip of the damage is localized and the damage size is computed as the area of the polygon formed by these tips. This method has been applied on a CFRP composite plate numerically and experimentally (Sorrentino and De Fenza, 2017a) and numerically on a plate with stiffeners (Sorrentino and De Fenza, 2017b). Migot et al. proposed a quantification strategy to assess the size of a crack (by localizing the tips of a crack and measuring the distance between them) and a hole (localizing the edge of the hole and measuring its diameter using two different imaging techniques). An application has been done on an aluminum plate (Migot et al., 2019). A data-driven approach was proposed by Kulakovskyi using a Convolutional Neural Networks trained on a dataset composed of images generated by simulation with spectral finite element method and a localization algorithm called Excitelet (Quaegebeur et al., 2011). In this dataset, an aluminum plate contained a hole with various sizes and positions. Once the model performs well on this training set, it is applied on unknown datasets, one with numerical data generated the same way as the set used for training, and an experimental dataset (Kulakovskyi, 2019). Another way to predict the size of a damage is to find a Damage Index (DI) that varies in a monotonic manner with the size of the damage. In (Giridhara et al., 2010), the authors introduced a DI based on wavelet coefficients that verifies this condition. It has been applied to a hole damage with several diameters, on an aluminum plate. However, no prediction of unknown damage was done in this paper.

In these articles, only one method of localization is applied, often with isotropic materials such as aluminum and on simple geometries like plates. In addition, applications are made with artificial damages as holes or slits, whereas there were very few on delaminations. Besides, there is no universal quantification method in the literature that can post-process images from different localization techniques and compare the results with each other. The approach proposed in this paper consists in monitoring the growth of a damage based on the computation of a feature that varies in a monotonic manner with the actual size of the damage. This feature is extracted from damage localization methods results: it corresponds to the area of high index regions in images returned. This feature is computed for each

element of a training set composed of previous damaged states of the structure. Then a data-driven model is built with a polynomial regression. Finally, one can assess the size of an unknown and larger damage. Results of this method are compared for four different damage localization techniques: ToA, TDoA, DAS, and RAPID. As more and more aeronautic structures are made of composite materials (Hexcel, 2013), a reliable quantification method must be tested on this type of material. Hence, the applications in this paper are made on CFRP specimen. The originality of this work consists in post-processing the results of existing localization methods to estimate the size of the damage. Moreover, an application to transfer learning is proposed. It involves to learn the quantification model on a full dataset available for a sample and use the inferred model to predict the size on another similar coupon.

After reviewing the different damage localization methods used in this paper, the proposed approach is explained in details. A method to automatically select its own parameters is proposed. Preliminary tests are made on numerical simulation data to assess the sensitivity of the method to input frequency and damage localization algorithms. The approach is successfully validated on experimental data coming from CFRP plate samples equipped with a piezoelectric transducers network. Two types of process for close to real life delamination generation are studied: fatigue testing and laser shock. Finally, a demonstration where the algorithm is used to learn on a composite plate and prediction is done on another sample, is made.

2. Proposed damage quantification strategy

2.1. Investigated damage localization methods

Damage localization methods are algorithms that take as input raw signals from piezoelectric transducers bonded on a composite structure. These raw signals are first denoized, filtered and time-aligned. The group velocity of the ultrasonic Lamb waves is then computed. The outputs of these algorithms are the estimated position of the damage (if there is one) and a map of the structure where each pixel is associated with a Damage Localization Index (DLI). The higher is this value, the higher the damage is likely to be localized at this position. The point with the maximum DLI is considered as the estimated position of the damage. The damage localization methods investigated in this paper are briefly described in the following sections. In the rest of the section, M_{PZT} denotes the number of piezoelectric elements.

2.1.1. Time of Arrival (ToA). Time of Arrival (ToA) method is a multilateration technique widely used for damage localization purposes. We consider an actuator i, a sensor j and a damage at the coordinates (x, y). The method consists in computing the difference of time of flight of the wave packet on the direct path (actuator-sensor) and on the secondary path (actuator-damage-sensor) denoted as $\mathrm{ToA}_{ij}(x, y)$

$$\mathrm{ToA}_{ij}(x,y) = \frac{\sqrt{(x_i - x)^2 + (y_i - y)^2}}{c_g} + \frac{\sqrt{(x_j - x)^2 + (y_j - y)^2}}{c_g} - \frac{\sqrt{(x_i - x_j)^2 + (y_i - y_j)^2}}{c_g} \quad (1)$$

where (x_i, y_i) and (x_j, y_j) are respectively the coordinates of the actuator i and the sensor j. c_g is the group velocity. The possible locations of the damage causing the diffracted signal are lying on a locus drawing an ellipse. The implementation of this algorithm described in (Fendzi et al., 2016) is used here. The structure under study is spatially sampled and the theoretical ToA $t_{ij}^{th}(x, y)$ is computed for each pixel (x, y) and each path $i - j$. Then a damage localization index is obtained at each point of the structure by comparing the theoretical time of flight $\mathrm{ToA}_{ij}^{th}(x, y)$ with the one extracted from scattered signal $\mathrm{ToA}_{ij}^{xp}(x, y)$ as stated in equation (2).

$$\mathrm{DLI}_{\mathrm{ToA}}(x,y) = \sum_{i=1}^{M_{\mathrm{PZT}}-1} \sum_{j=i+1}^{M_{\mathrm{PZT}}} e^{-\frac{1}{\tau}\left|\mathrm{ToA}_{ij}^{th}(x,y) - \mathrm{ToA}_{ij}^{xp}(x,y)\right|} \quad (2)$$

where τ is a focus parameter introduced in order to reduce the influence of secondary reflections of the scattered signal.

2.1.2. Time Difference of Arrival (TDoA). Time Difference of Arrival (TDoA) is based on the same principle as ToA. The only difference is that in this method a group of three piezoelectric elements is considered: one actuator i and two sensors j and k. For each point (x, y) the theoretical difference of the ToA at each sensor is computed and compared with the difference extracted from the scattered signal. As in the ToA method, a focus parameter τ is introduced to limit the influence of secondary reflections.

2.1.3. Delay and Sum (DAS). In the Delay-and-Sum method (DAS) (Michaels, 2008) for each point (x, y) of the structure under interest, time of arrival $t_{ij}(x, y)$ of the Lamb waves is estimated for the secondary path actuator i to (x, y) and (x, y) to sensor j. The residual of this signal $r_{ij}(t)$, that is, the difference of magnitude between the reference signal and the one that is tested, is then computed. Each residual $r_{ij}(t)$ is shifted by $t_{ij}(x, y)$.

$$s(t;x,y) = \frac{1}{N} \sum_{i=1}^{M_{\mathrm{PZT}}-1} \sum_{j=i+1}^{M_{\mathrm{PZT}}} r_{ij}\big(t - t_{ij}(x,y)\big) \quad (3)$$

For each tested point, the resulting signal difference is averaged over each actuator-sensor path as shown in equation (3). The damage index is then computed by integrating the square of the signal difference over a time window.

$$\mathrm{DLI}_{\mathrm{DAS}}(x,y) = \int_{K\Delta t} [s(t;x,y)]^2 \mathrm{d}t \tag{4}$$

It can be noticed that in the integral the time reference is the nominal arrival time for location (x,y). K is an integer denoting the number of time steps Δt over which time integration is performed.

2.2. Reconstruction Algorithm for the Probabilistic Inspection of Damage (RAPID)

The Reconstruction Algorithm for the Probabilistic Inspection of Damage (RAPID) (Zhao et al., 2007) consists in computing the probability of a defect occurrence using the relative amplitude of the signal change on each actuator-sensor path. This probability P_{ij} is computed using the signal difference coefficient $A_{ij} = 1 - \rho_{ij}$ (with ρ_{ij} the correlation coefficient between the actuator i and the sensor j) and a ratio representing how far is the point from the direct path. For each actuator-sensor path, a distribution function is drawn to represent this property. Here an elliptical distribution is used and its spread is controlled by a scalar parameter β.

$$P_{ij} = A_{ij}\left[\frac{\beta - R_{ij}(x,y)}{\beta - 1}\right] \tag{5}$$

with

$$R_{ij}(x,y) = \begin{cases} \mathrm{RD}_{ij}(x,y) & \text{when } \mathrm{RD}_{ij}(x,y) < \beta \\ \beta & \text{when } \mathrm{RD}_{ij}(x,y) \geq \beta \end{cases} \tag{6}$$

where

$$\mathrm{RD}_{ij}(x,y) = \frac{d_{AP} + d_{PS}}{d_{AS}} \tag{7}$$

d_{AP} is the distance actuator to point (x,y), d_{PS} the distance point (x,y) to sensor and d_{AS} the distance between the actuator and the sensor. The DLI within the sensor network is then expressed as a linear summation of the P_{ij} values of every pair as shown in equation (8).

$$\mathrm{DLI}_{\mathrm{RAPID}}(x,y) = \sum_{i=1}^{M_{\mathrm{PZT}}-1} \sum_{j=i+1}^{M_{\mathrm{PZT}}} P_{ij} \tag{8}$$

2.3. HDLI feature computation

All the damage localization methods presented previously provide a map of DLI over the structure under study that will be processed to compute a quantification feature. For each damage localization method, these maps are normalized by the highest DLI value in the whole training set. The idea is then to compute a single feature that varies with the damage size in a monotonic manner. From Figure 1(a) which constitutes a typical DLI map, it can be observed that there is a region where the DLI is higher than the rest of the image, without clear boundaries. The assumption made here is that the area of this region is a function of the actual damage size. Applying a threshold T to a DLI map gives a binary image where one or several regions with a DLI above the threshold can be identified. The next step consists in isolating the region surrounding the estimated damage position (i.e. the position with the maximum DLI).

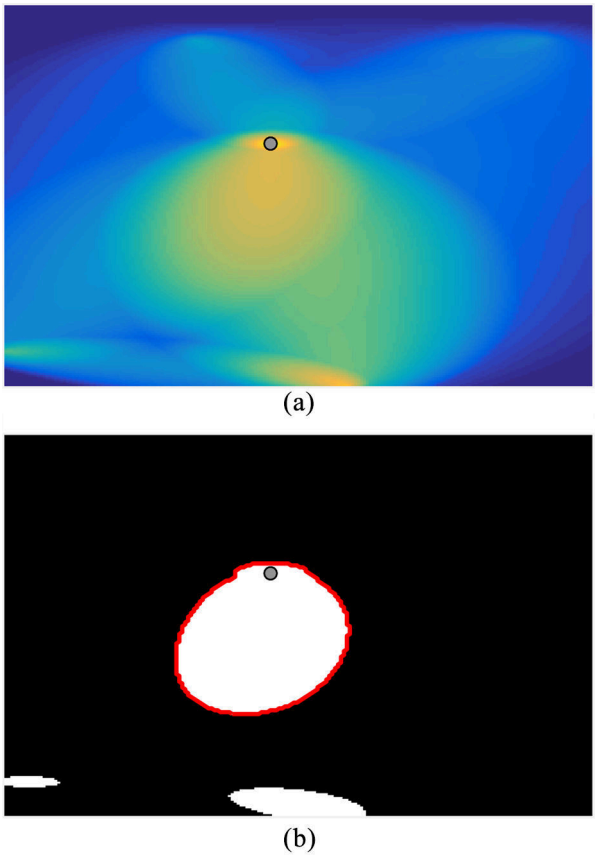

Figure 1. Damage localization results (a) and the binary image obtained after applying a threshold function (b).
The gray circle is the estimated damage localization.

The Moore-Neighbor image segmentation algorithm (Rafael et al., 2002) is used to perform this task. It consists in identifying the boundaries of all the objects in a binary image. Beginning at a starting pixel called current pixel, the algorithm visits each pixel in the starting pixel's neighborhood (i.e. the eight pixels that share a vertex or an edge with the current pixel) in clockwise direction. If a pixel belonging to an object is detected, it becomes the new current pixel. The procedure continues until matching the stopping criterion. The criterion

used in this paper (as it is the one implemented in *MATLAB*) is called Jacob's stopping criterion. It states that the algorithm stops after entering the starting pixel a second time in the same manner it has been entered initially.

The result of this threshold and segmentation steps is shown in Figure 1(b). The area of the isolated region is computed and denoted A. This area is divided by the total area A_{tot} of the structure under study in order to have a dimensionless damage index that will be called HDLI (High Damage Localization Index area) in the following.

$$\mathrm{HDLI} = \frac{A}{A_{tot}} \tag{9}$$

2.4. Damage quantification model training

In order to estimate the size of an unknown damage, a data-driven model is built. The workflow followed to infer and validate such a model is divided in two steps. The first one is the training step: it consists in training in a supervised manner a data-based model from a training set, that is, a collection of signals corresponding to different damage states with the corresponding size of the damage. In the prediction step, the size of an unknown and larger damage is predicted with the model previously inferred in order to validate its extrapolation performances.

2.4.1. Training step. Let's assume that a training set of N damage cases labeled with the associated damage size $\{(S_1, s_1), \ldots, (S_N, s_N)\}$ is available. S_i is the set of signals from the transducers for the i^{th} damage case and s_i is the corresponding size of the damage. This dataset is processed through a given damage localization method. Then one gets a new dataset $\{(I_1, s_1), \ldots, (I_N, s_N)\}$ where I_i is the image returned by the damage localization algorithm. Once the HDLI of each training example is computed the training set $\mathbf{X} = \{(h_0, s_0), \ldots, (h_N, s_N)\}$ is available. h_i is the HDLI described previously computed from the i^{th} image. HDLI values close to 0 are discarded to improve the sensitivity of the method for large damages since the purpose is to extrapolate a model toward higher damage sizes. In the following, $\boldsymbol{H} \in \mathbb{R}^N$ and $\boldsymbol{S} \in \mathbb{R}^N$ will denote respectively the vector of HDLI features and the vector of damage sizes of all N training samples. To predict the future size of the damage under study, it is necessary to build a model that fits well the data on the training set and that can be extrapolated. Since the HDLI does not vary linearly with the damage size, a classical linear regression cannot be used. For the sake of simplicity, a polynomial regression is chosen. This method has the advantage to fit the data well and does not occult the physics of the model like other supervised machine learning approaches. Polynomial regression is then performed on $\mathbf{X}$, and the j^{th} coefficient of the regression model is denoted β_j.

$$\hat{\boldsymbol{S}} = \sum_{j=0}^{d} \beta_j \boldsymbol{H}^j \tag{10}$$

In equation (10), d is the degree of the polynomial, $\hat{\boldsymbol{S}} \in \mathbb{R}^N$ is the vector of estimated damage size and $\boldsymbol{H}^j \in \mathbb{R}^N$ is the vector of j^{th} power of the components of $\boldsymbol{H}$. In order to keep the model variance low, a variation of classic linear regression called ridge regression is used (Friedman et al., 2001). It consists in adding a penalty term λ on the parameters β_i in the ordinary least square regression problem to control for their amplitude. The vector of regression coefficients $\hat{\boldsymbol{\beta}}$ must minimize the following equation:

$$\hat{\boldsymbol{\beta}} = \underset{\boldsymbol{\beta} \in \mathbb{R}^d}{\operatorname{argmin}} \left(\|\boldsymbol{S} - \boldsymbol{\beta}\boldsymbol{H}\|_2^2 + \lambda \|\boldsymbol{\beta}\|_2^2 \right) \tag{11}$$

The problem can be written under a matrix form:

$$\hat{\boldsymbol{\beta}} = \left(\boldsymbol{H}^T\boldsymbol{H} + \lambda \boldsymbol{I}\right)^{-1} \boldsymbol{H}^T \boldsymbol{S} \tag{12}$$

where $\boldsymbol{I}$ is the N-by-N identity matrix. The next step is to compute the optimal value for the penalty term λ_{opt} in order to minimize the error over the training set. To choose an optimal value for the penalty term λ_{opt}, a gradient descent algorithm is used to minimize the cost function J with respect to λ. To avoid overlearning the model on the training data set, this cost function is calculated using a cross-validation technique. This step limits the risk that the model gives very good results only on the training set while the predictions on the test set are poor.

$$\lambda_{\text{opt}} = \underset{\lambda \in \mathbb{R}}{\operatorname{argmin}}(J) \tag{13}$$

Since the dataset considered here is small, the cross-validation technique chosen here is called *Leave-One-Out*. It consists in training the model on a new training set where one of the example is left out. The error of the model is then computed for the example being left out

$$\begin{aligned} J_i &= \frac{1}{2}|s_i - \hat{s}_i|^2 + \frac{\lambda}{2}\sum_{k=1}^{d} \| \beta_k \|_2^2 \\ &\forall i \in [\![1; N]\!] \end{aligned} \tag{14}$$

This process is repeated for every item of the training set that is, N times. The cost function J used in the optimization problem equation (13) is computed as the mean of all J_i

$$J = \frac{1}{N}\sum_{i=1}^{N} J_i \tag{15}$$

One must choose a value for the degree of the polynomial. Any degree high enough will yield to the same regression model because coefficients relative to high degree terms will be close to zero thanks to the regularization equation (15). Throughout this paper, d is set to 8.

2.4.2. Prediction step. The data-driven model built earlier is then used to predict the size of an unknown and larger damage. The first step is to process the signal with the damage localization method to get a DLI image of the structure. Then the HDLI h_{test} is computed from this image. The corresponding size s_{test} is finally estimated using the size quantification model previously built according to:

$$\hat{s}_{\text{test}} = \sum_{k=0}^{d} \hat{\beta}_k h_{\text{test}}^k \tag{16}$$

2.5. Methodology

The overview of the method is depicted in Figure 2. M_{PZT} stands for the number of piezoelectric elements, M_{rep} stands for the number of measures for the same damage case and N is the size of the training set. The steps to follow are

Step 1 Get signals from each transducer on the plate.
Step 2 Process the signals corresponding to the i^{th} case with one of the damage localization algorithm described earlier. The result is a DLI image of the structure.
Step 3 Compute the HDLI associated with the image i.
Step 4 Repeat steps 2 and 3 for each $i \in [\![1; N]\!]$.
Step 5 Perform the polynomial regression model using the training set of HDLI previously computed and the known damage size of the corresponding damage case.
Step 6 Compute the HDLI value of an unknown damage case.
Step 7 Use the regression model to estimate the size of the damage.

In order to assess the performance of the inferred model, the following metric will be used in the rest of this paper. It is defined as the relative error computed on training or test set

$$\varepsilon = \frac{1}{n} \sum_{l=1}^{L} \frac{|\hat{s}_l - s_l|}{s_l} \tag{17}$$

where L is the size of the dataset.

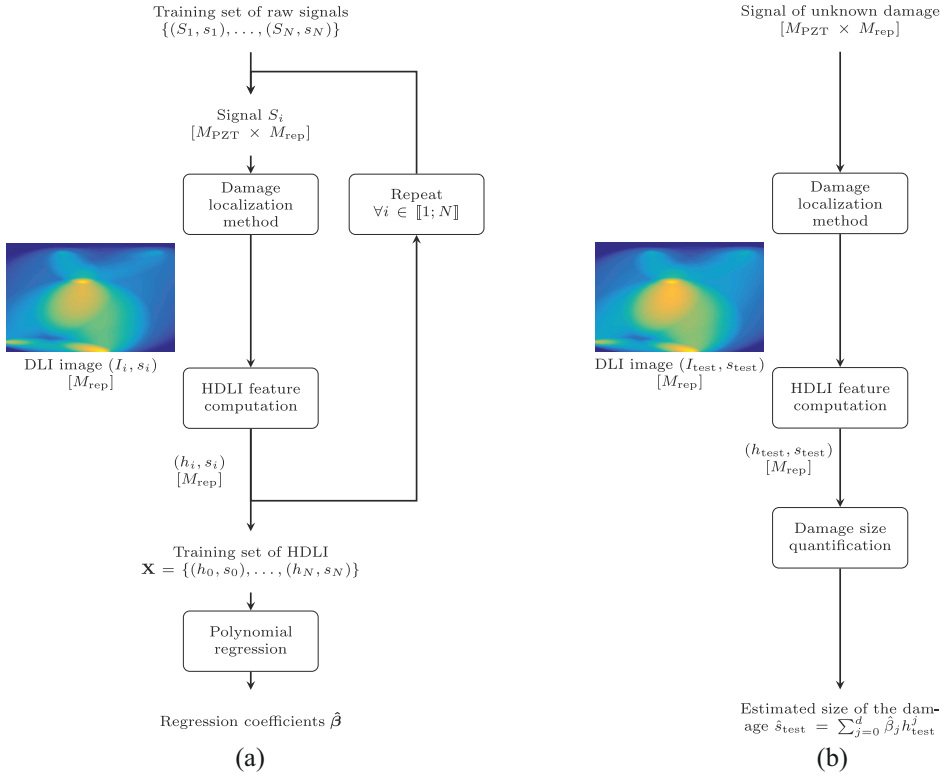

Figure 2. Overview of the damage size quantification algorithm based on the post processing of damage localization algorithms. Description of the training step (a) and the prediction step (b).

Table 1. Localization parameters selected.

Localization method	Method parameter	Symbol	Selected value
ToA and TDoA	Decay rate of an exponential windowed function applied to reduce secondary reflections.	τ	5.0×10^{-6}
DAS	Number of samples over which time integration is performed.	K	1
RAPID	Parameter set to adjust the spread of the ellipses around each path.	β	1.05

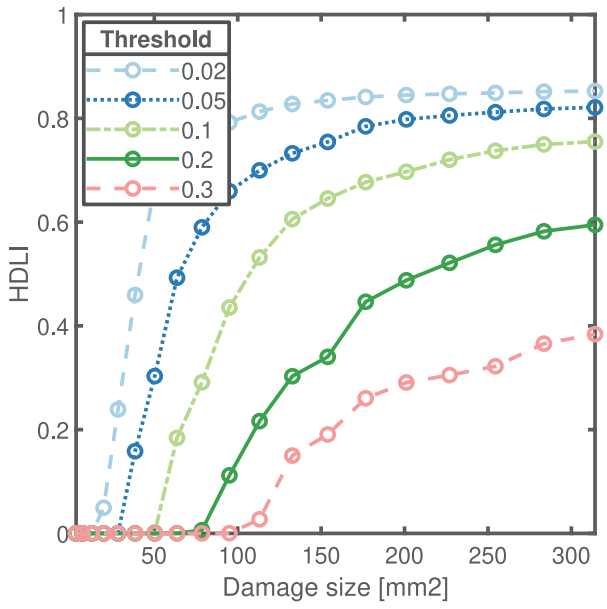

Figure 3. HDLI sensitivity to threshold parameter using RAPID localization method.

2.6. Parameters selection for damage quantification

As previously explained, the damage quantification method proposed in this paper is tested with several damage localization methods: ToA, TDoA, RAPID, and DAS. For each of these algorithms, a tuning parameter has to be chosen. In the ToA and TDoA algorithms, an exponential window function is introduced to reduce the effect of secondary reflections (Fendzi et al., 2016). This function depends on a decay rate τ (see equation (2)). The DAS algorithm depends on the number of samples K over which time integration is performed (Michaels, 2008). In the RAPID approach the user can set a parameter called β corresponding to the spread of the ellipses around each path (Sharif-Khodaei and Aliabadi, 2014). Moreover, the post-processing method presented in this paper also depends on the threshold level T in the HDLI feature computation step.

In order to have an unique damage size for one HDLI, parameters need to be chosen to get a bijection between HDLI and damage size values. The tuning parameters for the localization algorithms used throughout this work are given in Table 1. These values have been set empirically.

The only parameter left to be selected is the threshold T. In order to illustrate the influence of this parameter on the obtained results, sensitivity of the RAPID algorithm to threshold is depicted Figure 3. One can observe that some threshold values lead to bijective function that can be used for damage size prediction whereas some others parameters values provide the same damage size for a wide range of HDLI and thus do not allow *a priori* for reliable damage size quantification. Thus, to get a threshold value that is compatible with the post-processing method described earlier, the optimal threshold T_{opt} minimizing the following cost function over the training set is selected:

$$T_{\text{opt}} = \underset{T\in\mathbb{R}}{argmin}\left(\frac{1}{2N}\sum_{i=1}^{N}\| s_i - \hat{s}_i\|^2\right) \qquad (18)$$

Unfortunately, this cost function is not smooth and its derivative cannot be computed analytically. Moreover, many different local minima could exist. To find a threshold providing an acceptable error on the training set, one uses a minimization algorithm repeated several times with a random initialization. The retained threshold T_{opt} is the one with the lowest associated value of the cost function. The simplex method (Lagarias et al., 1998), which is a derivative-free optimization technique, is used.

3. Application of the proposed damage quantification method

3.1. Preliminary tests on simulation data

A preliminary test is done on data coming from numerical simulation to assess the performance of the method in the case of a damage with well-defined boundaries. Another objective is to study the influence of the excitation signal central frequency on quantification results.

The structure under consideration is a stiffened composite panel made of graphite-epoxy plies with the stacking sequence [45°/0°/45°/90°/−45°/0°]. The properties of one ply are given in Table 2. The structure is equipped with five NCE51 piezoelectric elements each with a diameter of 20 mm and thickness of 0.1 mm. The FEM model of the structure with piezoelectric elements and highlighting damage position is shown in Figure 4. The localization algorithms used here assume

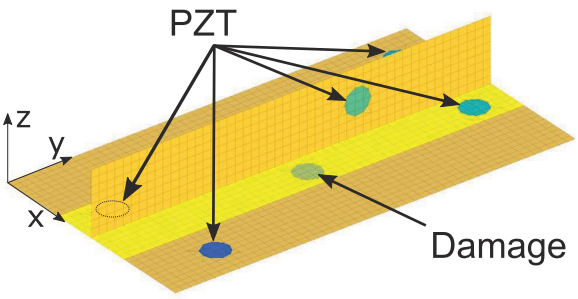

Figure 4. FEM model of the stiffened panel used for simulation.

Table 2. Mechanical properties used for numerical simulation.

Density [g/cm ^{3}]	E_0 [GPa]	E_{90} [GPa]
1.57	163	10

a 2D structure. We therefore project the position of the PZT located on the stiffener in the plane $z = 0$ to consider only the coordinates x and y. Piezoelectric elements and simulated damage coordinates can be found in Table 3. Signal used is a five-cycles tone burst with 10 V amplitude. Random noise is added to introduce variability in the data with a signal to noise ratio of 70 dB. The simulation has been performed with three different signal with central frequency of 120, 140, and 160 kHz. For each damage case 10 repetitions have been proceeded. For any damage localization algorithm, each repetition is compared to each repetition of the healthy state leading to 100 DLI maps per damage case.

The model is meshed with 1 mm $\times$ 1 mm square shell elements. The guided wave excitation and sensing is modeled with piezoelectric Mindlin shells, taking into account the viscoelasticity of the composite core, the glue, and the piezoelectric coupling equations. Electrical degrees of freedom are included in addition to the nodal displacement (Balmes and Deraemaeker, 2013; Balmes et al., 2014). The mesh size was chosen to be compatible with the wavelength of the S_0 mode at 160 kHz (40 mm), leading to 40 elements per wavelength which ensure mesh convergence. Only the S_0 mode is considered in here since it is the one used in the localization algorithms studied. Even if this mode is less sensitive to delamination than the A_0 mode, it propagates faster. This avoids confusing the wave packet coming from the damage with reflections on the edges of the structure. Since the other frequencies studied here have higher wavelength, the same mesh will be use for all frequencies. The time step for the transient simulation is 0.5 μs leading to a sampling frequency of 2 MHz. The numerical simulation is done with *MATLAB* toolbox SDT (Balmes and Deraemaeker, 2013) using an explicit Newmark method. More details of simulation guidelines of Lamb waves can be found in (Shen and Giurgiutiu, 2016).

The simulated damage has a circular shape with a radius varying from 1 to 10 mm by step of 0.5 mm leading to 19 different damage cases. The delamination is modeled by a decrease of the Young modulus of 90% in the damaged area. This kind of model has been compared to experimental results (Kim et al., 2007). It is shown that the delamination indeed induces a local stiffness reduction. Even if this model does not fully account for the non-linear behavior of the delamination, it will be realistic enough to perform preliminary tests.

A healthy case that is, without any damage is used as reference by the damage localization algorithms. The first 70% of this dataset is used as training set (from 1 to 7 mm) and the 30% left (from 7.5 to 10 mm) are used as testing set in order to assess the prediction performance of the damage quantification model. In an industrial context it corresponds to measure the size of the damage in its early life when it is not yet an issue for the integrity of the structure. This learning dataset is used to build a quantification model. Then the prediction relies on the extrapolation of this model to upcoming larger sizes of the damage. Thus, it is possible to know when the delamination reaches a critical size that threaten the integrity of the structure.

3.2. Application to fatigue experimental data

The post-processing strategy is also applied to experimental data coming from fatigue test carried out on CFRP specimens conducted jointly by NASA and Stanford University (Saxena et al., 2011).

The specimens under study are CFRP composite plate with a dogbone shape and a notch at mid-length which geometrical dimensions can be found in Figure 5. The specimen is equipped with 12 piezoelectric elements bonded on the surface, that is, a six-PZT-sensor SMART Layer© from Acellent Technologies, Inc. on each side of the coupon. The transducers placed at the top of the coupon are used as actuators whereas the bottom piezoelectric elements are exclusively used as

Table 3. Location of center points of PZT and of damaged area.

	PZT1	PZT2	PZT3	PZT4	PZT5	Damage
x [mm]	50	25	275	275	200	150
y [mm]	25	98.8	140	66.3	82.5	66.3

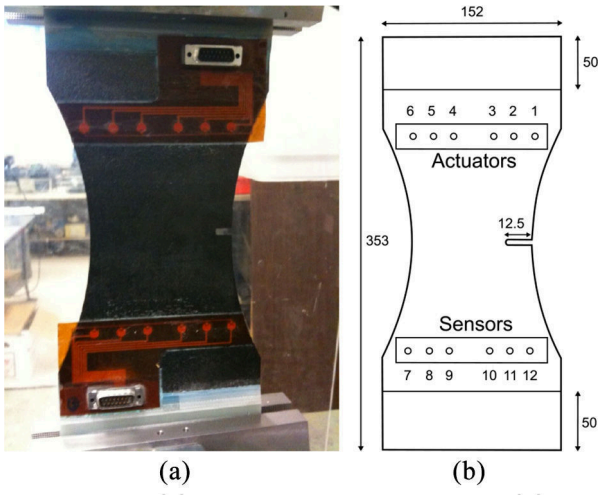

Figure 5. (a) CFRP samples used in NASA dataset, (b) Dimensions of the coupons in mm.
Adapted from Larrosa et al. (2014).

sensors. This leads to a total of 36 actuator-sensor paths. The experimental protocol consists in running a cycling tension-tension fatigue test. The presence of the notch induces a stress concentration that creates a delamination growing with the number of cycles. These fatigue tests were performed on a MTS machine with frequency of 5 Hz and a stress ratio of $R = 0.14$. The test was regularly interrupted to perform Lamb waves pitch-catch acquisition. The excitation signal used is a 5-cycles tone burst with a central frequency of 250 kHz and an amplitude of 50 V. The frequency is chosen to be the one where fundamental symmetric and antisymmetric are the most distinguishable as mentioned by (Larrosa et al., 2014). An X-ray image is also taken at each interruption to visualize the size of the delamination Figure 6. Several layups are available in this dataset. In this paper the layups L1 and L2 had been retained with respectively the stacking sequences $[0_2/90_4]_s$ and $[0/90_2/45/-45/90]_s$. With these layups a delamination can be visualized growing progressively with the number of cycles, allowing a supervised machine learning approach. The dataset is split in one training set (first 70% of damage cases) and one test set (30% of other damage cases). Each damage case is composed of raw data from piezoelectric patches. Actual delaminations area were extracted from X-ray images with the image processing software Digimizer[1].

3.3. Application to laser shocks delamination experimental data

The proposed approach is applied on another type of delamination. This time the damage is generated with symmetrical laser shocks. When a laser pulse of short duration (few nanoseconds) and high power reaches the surface of the plate, the first few micrometers of the

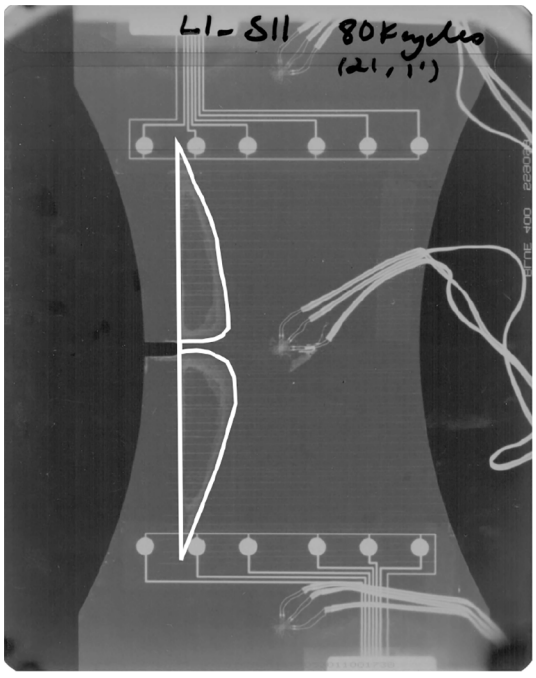

Figure 6. X-ray image of specimen L1 S11 taken at 80 kcycles. The edges of the delamination are highlighted in white.

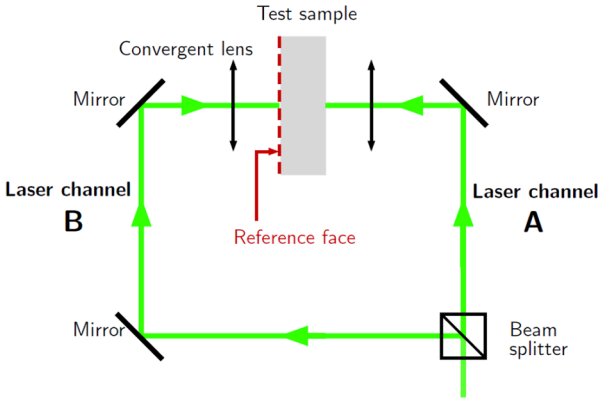

Figure 7. Experimental setup in case of symmetrical laser shock (Ghrib et al., 2017).

impacted area are transformed into plasma which expands rapidly against the target surface. In the current experimental setup, a sacrificial layer made of aluminum is placed on the target to avoid the damaging of the plate. This plasma expansion release creates a shock wave into the composite plate. In the symmetrical configuration, each face of the plate is irradiated with a laser beam generating two shock waves propagating in opposite direction through the thickness as can be seen in Figure 7. The crossing of the two waves creates local high tensile stress which can result in damage at a through thickness depth if the energy level of the laser irradiation is high enough. More details about controlled delaminations in composites can be found in Ghrib et al. (2017).

Table 4. Mechanical properties used for laser shocks delamination experiments.

Density [g/cm ^{3}]	E_{11} [GPa]	E_{22} [GPa]	E_{12} [GPa]	$G_{13} = G_{12}$ [GPa]	ν_{12}
1.594	140	9	4.5	4.5	0.3

The specimens under study are CFRP composite plates with dimensions of 300 mm $\times$ 400 mm $\times$ 2.2 mm and the following stacking sequence $[0/90/0/90/0/90/0/90]_s$. The ply properties are shown in Table 4. Five PZTs NCE51 are bonded to each coupon with a Redux 322 glue.

A pristine sample is used as a reference state whereas three other plates are damaged with different energy levels, leading to different delamination sizes. An ultrasound non-destructive test had been carried out on each sample and revealed that the delaminations generated are 7, 14, and 21 mm length. The first two damage cases are used as training set and the remaining one is considered as a test set.

The excitation signal used in this application is a five-cycles tone burst with a central frequency of 140 kHz and an amplitude of 10 V.

4. Results

For each considered structure and each damage localization method, performances of the proposed damage quantification algorithm are evaluated by two means. The first one is a plot where the X axis is the true size of the delamination area and the Y axis is the size predicted by the damage quantification algorithm. The $y = x$ line represents a prediction without error: the closer a value is to this line, the better the prediction. As stated previously, for each structure considered, the dataset is split into a training set (the first 70% of the damage cases) and a testing set (the last 30% of the damage cases). The other way to assess the performance of the strategy proposed in this paper is to compute the error on the training set and the test set of each structure.

Figure 8 shows performance of the damage size prediction on simulation data for the four damage localization algorithms studied in this paper. Only the 140 kHz excitation signal is considered here AToA and TDoA exhibit poor results on both training and testing dataset. DAS performs well on the training set although the prediction on the testing set is far from the true size. The RAPID algorithm provides the best results on both training set and testing set as the predicted values are very close to the $y = x$ line. In the following, only the RAPID method will be used. Moreover, the performance of DAS and RAPID methods does not seem sensitive to noise.

Figure 9 presents the quantification results when applied to L1 and L2 experimental specimens. The RAPID method gives promising results on both training set and testing set for each type of layup. These observations are confirmed by Table 5 which shows the error on the training set $\varepsilon_{\text{train}}$ and on the test set $\varepsilon_{\text{test}}$ in order to assess the performance of the approach for each localization method. One can observe that qualitative remarks made about the plots are confirmed quantitatively here.

The laser shock dataset is very small ans sparse but as presented in Figure 10, the prediction giving with the RAPID method is close to the reality.

The influence of the excitation signal frequency on the prediction has been investigated. Figure 11 shows the sensitivity performance to the excitation frequency on the numerical dataset. In the same manner, at 140 kHz it is clear that the prediction is better than with others excitation frequencies. On the other hand, Figure 12 relates the prediction error $\varepsilon_{\text{test}}$ on the coupon L1 S11 for each frequency available in the dataset and for several learning rate that is, several sizes of training set. Each rate corresponds to the percentage of the whole dataset used as training set. It can be seen that the prediction error is the lowest for an input signal at 250 and 300 kHz. Table 6 shows that this tendency can be observed for most of L1 samples. This confirms the choice made earlier of a 250 kHz excitation frequency. Moreover, one can see that the optimal frequency is not sensitive to the learning rate.

5. Discussion

For both simulated and experimental data, the influence of the selected damage localization method is clear. HDLI computed with ToA or DToA shows no correlation with the true damage size leading to poor performance over training set and testing set. It could be explained by the fact that these methods only deal with time of arrival of the signal which is not influenced by the size of the damage. Another reason of this poor performance could also be the shape of the high DLI area which has a great influence on the quality of the regression. In the ToA and DToA, this region is made up of ellipses or hyperbolas which area does not clearly vary with the damage size as mentioned earlier in this paper. Besides, DAS and RAPID both exhibit great results on the training set. This performance could be explained by the fact that DAS and RAPID take amplitude of the signals into account in addition to time of flight, which make the HDLI more influenced by the size of the damage. Moreover, high DLI area in the

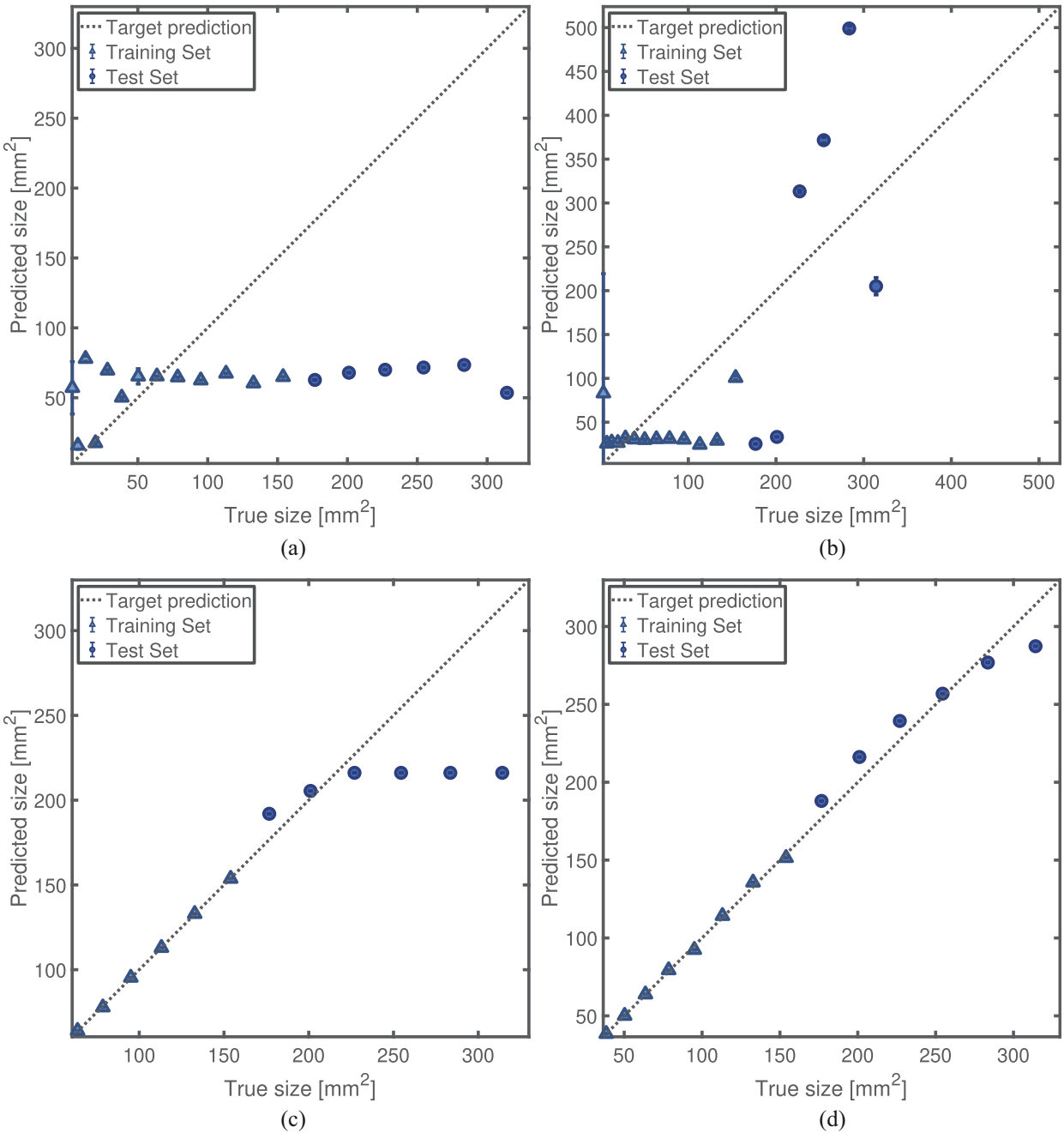

Figure 8. Damage quantification performance using different damage localization methods on numerical data. ToA (a), DToA (b), DAS (c), and RAPID (d).
The central frequency of the excitation signal is 140 kHz. The diagonal $y = x$ line correspond to a prediction without error.

DAS and RAPID methods is circular and HDLI varies in a monotonic manner over the size of the damage which lead to a more accurate model. It can also be noticed that with DAS and RAPID methods, the HDLI is close to zero for small damage sizes (usually under 4 mm). It would suggest an existence of a lower bound in damage size sensitivity for a given threshold T value. DAS method shows poor results on testing set. Indeed, above a certain level, the HDLI remains steady with the damage size. It means that above this level, each damage size leads to the same HDLI.

So far in this article we have only considered the case where the training step was done on the same sample as the prediction. However, even if we have seen earlier that this approach allows to infer a model with good results on the test set, another way to predict the size of an unknown damage is to perform the training step on the full dataset of a coupon to infer a more accurate model. The established model is then applied to a damaged coupon with the same parameters (geometry, material, PZTs positions) to predict the size of the delamination. With this technique, the prediction is

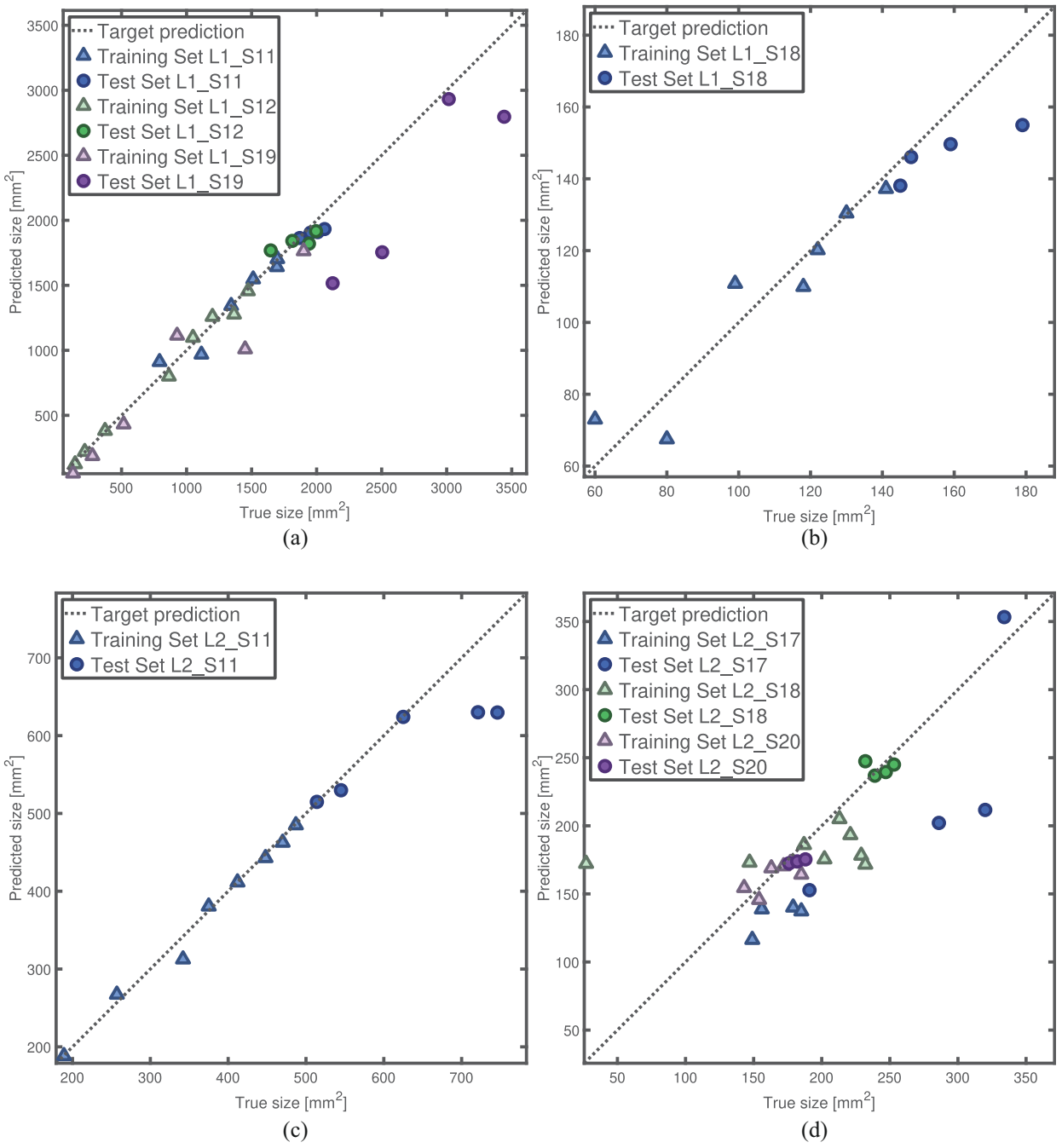

Figure 9. Damage quantification performance using RAPID method on NASA data: L1 coupons (a) and (b), L2 coupons (c) and (d). The diagonal $y = x$ line correspond to a prediction without error.

not made by extrapolating the model on unknown data but by evaluating the model on HDLI values similar to the training data, limiting the risk of error induced by extrapolating a polynomial model outside the training range. Moreover, this approach is closer to the industrial context since it does not require to have a training dataset for each coupon to be tested. This approach has been tested on the L1 S11, L1 S12, and L1 S19 coupons of the NASA dataset. For each one of the three coupons, the training step was performed on the specimen in question. A prediction test was performed on each of the remaining coupons, leading to a total of six possible combinations where prediction error can be found in Table 7. An example of these results is shown in Figure 13. For this set of coupons we obtain good results for some combinations, which shows that this method is encouraging. However, in this example this technique is not very robust since in some cases the method performs poorly. These results could be due to the lack of variety in the data. Indeed, for each damage

Table 5. Performance over the different datasets measured with training and test error in percent.

Dataset	ToA		DToA		DAS		RAPID	
	ε_{train}	ε_{test}	ε_{train}	ε_{test}	ε_{train}	ε_{test}	ε_{train}	ε_{test}
Numerical	510.0	73.0	340.0	37.0	7.5	13.0	1.4	3.1
Laser shock	94.0	189.0	78.0	56.0	8.9	75.0	112.0	7.7
L1 S11	200.0	32.0	140.0	36.0	36.0	31.0	12.0	7.8
L1 S12	220.0	50.0	300.0	70.0	62.0	38.0	13.0	6.2
L1 S18	390.0	49.0	410.0	36.0	31.0	20.0	19.0	7.8
L1 S19	750.0	85.0	400.0	78.0	29.0	47.0	38.0	27.0
L2 S11	410.0	52.0	420.0	55.0	6.9	15.0	3.6	5.6
L2 S17	24.0	31.0	55.0	37.0	8.4	9.8	19.0	25.0
L2 S18	110.0	3.9	110.0	20.0	160.0	33.0	150.0	5.0
L2 S20	12.0	29.0	77.0	11.0	5.2	4.2	10.0	3.5

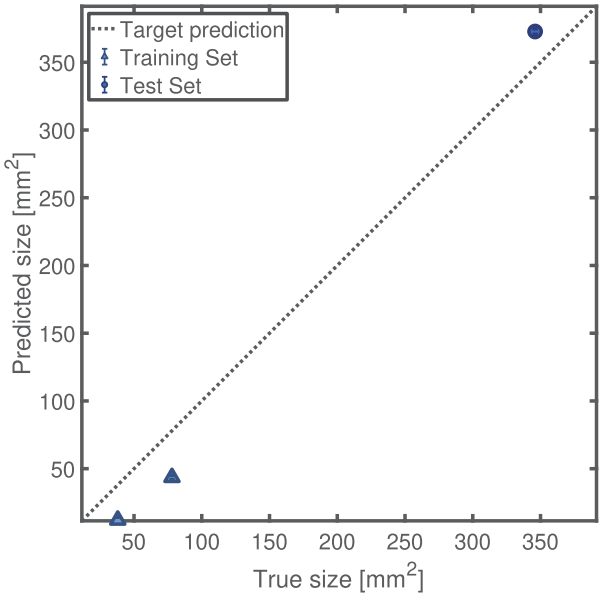

Figure 10. Damage quantification performance using RAPID method on laser shocked composite specimen.
The diagonal $y = x$ line correspond to a prediction without error.

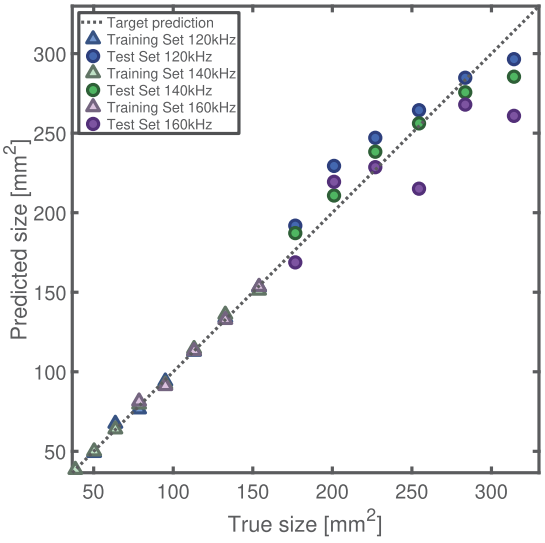

Figure 11. Performance sensitivity to the excitation frequency using RAPID localization method on numerical data.

case, only one measurement has been made, which does not allow to know the sensitivity of the acquired signals to noise. Another possible explanation is that the training is carried out on a single coupon. A training of the model on data from different coupons and multiple measurements for each damage case should limit the influence of the variation of the experimental, geometrical and material parameters and thus improve the reliability of this approach.

6. Conclusion

In this paper, a damage quantification strategy based on post-processing of damage localization results has been presented. Such a method allows for damage size assessment of a delaminated area by post-processing the images produced by damage localization algorithms

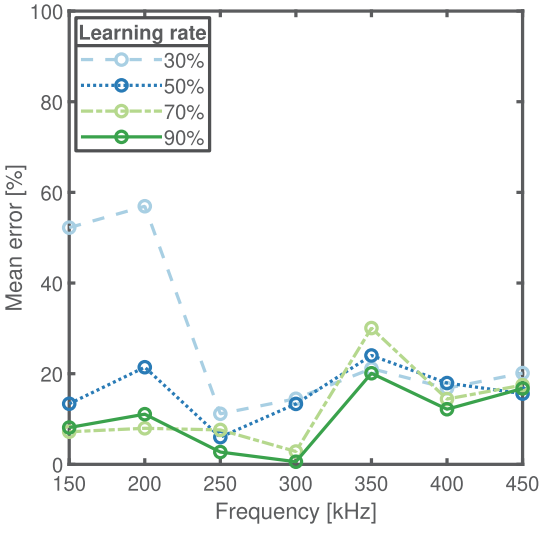

Figure 12. Influence of the excitation signal frequency on the prediction error for the sample L1 S11 using RAPID localization method.

Table 6. Influence of excitation signal frequency on the prediction error. For each frequency, the prediction error in percent on each NASA L1 samples is computed.

Frequency [kHz]	L1 S11	L1 S12	L1 S18	L1 S19
150	8.29	1.50	9.39	26.83
200	6.80	7.52	25.09	28.82
250	7.80	4.63	6.48	19.04
300	2.90	20.39	14.96	18.29
350	31.13	20.40	27.49	16.52
400	14.66	22.17	20.08	16.16
450	19.92	28.37	24.15	13.13

Table 7. Prediction error in percent of the transfer learning approach on NASA L1 coupons.

Frequency [kHz]	L1 S11	L1 S12	L1 S19
L1 S11	–	14.1	31.6
L1 S12	10.6	–	34.9
L1 S19	30.2	25.2	–

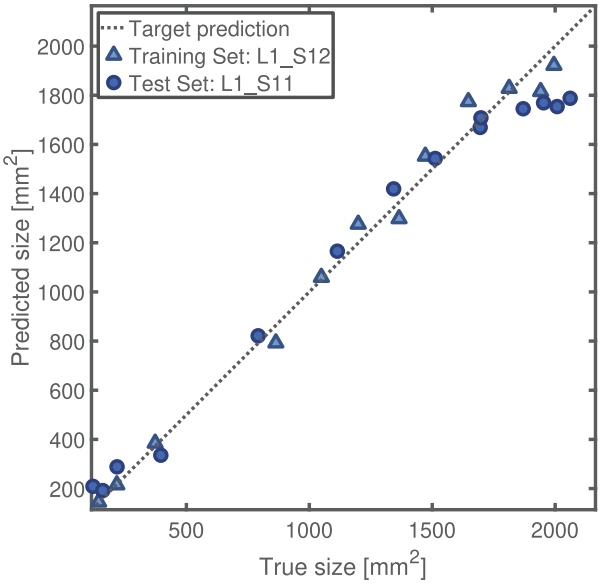

Figure 13. Transfer learning applied to L1 NASA samples. Here the train set is the dataset L1 S12 and the test set is the dataset L1 S11.

such as ToA, TDoA, DAS, and RAPID. From these images, a region of high localization index can be identified around the estimated damage location. The area of this region can be computed and used as a damage size sensitive feature. A data-driven model representing the mathematical relationship between this feature and the actual size of the damage is then inferred using a polynomial regression. The proposed method exhibit promising results with the RAPID method on numerical simulation data carried out on CFRP plate samples equipped with a stiffener. Moreover, the method is also successfully tested on experimental data of fatigue tests from NASA. Furthermore, it is demonstrated that a model can be confidently learned on a given CFRP plate sample and transferred to predict damage size on another similar CFRP plate sample.

The post-processing step presented in this study only compare the current damage state to the pristine one. This approach does not make use of all the information available. Indeed, it could be possible to compare the current state to every known damage state and use this information to built a more robust model.

Declaration of conflicting interests

The author(s) declared no potential conflicts of interest with respect to the research, authorship, and/or publication of this article.

Funding

The author(s) disclosed receipt of the following financial support for the research, authorship, and/or publication of this article: This work has received funding from the European Unions Horizon 2020 research and innovation program under the REMAP project (grant agreement number 769288). https://h2020-remap.eu/

ORCID iDs

William Briand https://orcid.org/0000-0001-8087-2463
Marc Rébillat https://orcid.org/0000-0003-0469-8437

Note

1. https://www.digimizer.com/

References

Ackert SP (2010) Basics of aircraft maintenance programs for financiers. http://aircraftmonitor.com/uploads/1/5/9/9/15993320/basics_of_aircraft_maintenance_programs_for_financiers___v1.pdf

Ashwin U, Raja S and Sathyanarayana CN (2014) Formulation of 36-noded piezoelectric spectral finite element scheme with active/passive layers coupled by Lagrange multipliers. *Smart Materials and Structures* 23(8): 085017.

Balmes E and Deraemaeker A (2013) *Modeling structures with piezoelectric materials*. SDT tutorial. https://www.sdtools.com/pdf/piezo.pdf

Balmes E, Guskov M, Rebillat M, et al. (2014) Effects of temperature on the impedance of piezoelectric actuators used for SHM. In: *14th symposium on vibration, shock and noise (VISHNO)*. France, pp. 1–6.

Dafydd I and Khodaei ZS (2020) Analysis of barely visible impact damage severity with ultrasonic guided Lamb waves. *Structural Health Monitoring* 19(4): 1104–1122.

Fendzi C, Mechbal N, R'ebillat M, et al. (2016) A general Bayesian framework for ellipse-based and hyperbola-based damage localization in anisotropic composite plates. *Journal of Intelligent Material Systems and Structures* 27(3): 350–374.

Friedman J, Hastie T and Tibshirani R (2001) *The Elements of Statistical Learning: Data Mining, Inference, and Prediction*. New York: Springer series in statistics.

Ghrib M, Berthe L, Mechbal N, et al. (2017) Generation of controlled delaminations in composites using symmetrical laser shock configuration. *Composite Structures* 171: 286–297.

Ghrib M, Rébillat M, Vermot des Roches G, et al. (2018) Automatic damage type classification and severity quantification using signal based and nonlinear model based damage sensitive features. *Journal of Process Control* 83: 136–146.

Giridhara G, Rathod VT, Naik S, et al. (2010) Rapid localization of damage using a circular sensor array and Lamb wave based triangulation. *Mechanical Systems and Signal Processing* 24(8): 2929–2946.

Giurgiutiu V (2005) Tuned lamb wave excitation and detection with piezoelectric wafer active sensors for structural health monitoring. *Journal of Intelligent Material Systems and Structures* 16(4): 291–305.

Giurgiutiu V (2007) *Structural Health Monitoring with Piezoelectric Wafer Active Sensors*. Amsterdam, Netherlands: Elsevier.

Hexcel (2013) Hexcel ready to fly on the A350 XWB. *Reinforced Plastics* 57(3): 25–26.

Kim JH, Pierron F, Wisnom M, et al. (2007) Identification of the local stiffness reduction of a damaged composite plate using the virtual fields method. *Composites Part A: Applied Science and Manufacturing* 38(9): 2065–2075.

Kulakovskyi A (2019) *Development of a SHM system by elastic guided waves applied to aeronautic structures*. PhD Thesis, Universit'e Paris-Saclay, France.

Lagarias JC, Reeds JA, Wright MH, et al. (1998) Convergence properties of the nelder–mead simplex method in low dimensions. *SIAM Journal on Optimization* 9(1): 112–147.

Larrosa C, Lonkar K and Chang FK (2014) In situ damage classification for composite laminates using Gaussian discriminant analysis. *Structural Health Monitoring* 13(2): 190–204.

Liu Y, Fard MY, Chattopadhyay A, et al. (2012) Damage assessment of CFRP composites using a time–frequency approach. *Journal of Intelligent Material Systems and Structures* 23(4): 397–413.

Michaels JE (2008) Detection, localization and characterization of damage in plates with an in situ array of spatially distributed ultrasonic sensors. *Smart Materials and Structures* 17(3): 035035.

Michaels JE and Michaels TE (2007) An integrated strategy for detection and imaging of damage using a spatially distributed array of piezoelectric sensors. In: SPIE (ed) *Health Monitoring of Structural and Biological Systems*. San Diego: SPIE - International Society for Optics and Photonics, p. 653203.

Migot A, Bhuiyan Y and Giurgiutiu V (2019) Numerical and experimental investigation of damage severity estimation using Lamb wave–based imaging methods. *Journal of Intelligent Material Systems and Structures* 30(4): 618–635.

Peng T, Saxena A, Goebel K, et al. (2013) A novel Bayesian imaging method for probabilistic delamination detection of composite materials. *Smart Materials and Structures* 22(12): 125019.

Qiu L, Liu M, Qing X, et al. (2013) A quantitative multidamage monitoring method for large-scale complex composite. *Structural Health Monitoring* 12(3): 183–196.

Quaegebeur N, Masson P, Langlois-Demers D, et al. (2011) Dispersion-based imaging for structural health monitoring using sparse and compact arrays. *Smart Materials and Structures* 20(2): 025005.

Rafael C, Gonzalez SLE and Woods RE (2002) *Digital Image Processing Using MATLAB*. USA: Prentice Hall.

Saxena A, Goebel K, Larrosa CC, et al. (2011) CFRP Composites Data Set. https://ti.arc.nasa.gov/tech/dash/groups/pcoe/prognostic-data-repository/

Sharif-Khodaei Z and Aliabadi MH (2014) Assessment of delay-and-sum algorithms for damage detection in aluminium and composite plates. *Smart Materials and Structures* 23(7): 075007.

Shen Y and Cesnik CES (2017) Local interaction simulation approach for efficient modeling of linear and nonlinear ultrasonic guided wave active sensing of complex structures. *Journal of Nondestructive Evaluation, Diagnostics and Prognostics of Engineering Systems* 1(011008): 1–9.

Shen Y and Giurgiutiu V (2016) Combined analytical FEM approach for efficient simulation of Lamb wave damage detection. *Ultrasonics* 69: 116–128.

Sorrentino A and De Fenza A (2017a) Damage detection in complex composite material structures by using elliptical triangulation method. In: *The 11th International Workshop on Structural Health Monitoring*. Standford, USA: DEStech Publications, Inc.

Sorrentino A and De Fenza A (2017b) Improved elliptical triangulation method for damage detection in composite material structures. *Proceedings of the Institution of Mechanical Engineers, Part C: Journal of Mechanical Engineering Science* 231(16): 3011–3023.

Su Z and Ye L (2005) Lamb wave propagation-based damage identification for quasi-isotropic CF/EP composite laminates using artificial neural algorithm: Part II – implementation and validation. *Journal of Intelligent Material Systems and Structures* 16(2): 113–125.

Su Z and Ye L (2009) *Identification of Damage Using Lamb Waves: From Fundamentals to Applications*. Springer, London: Springer.

Wang J and Shen Y (2019) An enhanced Lamb wave virtual time reversal technique for damage detection with transducer transfer function compensation. *Smart Materials and Structures* 28(8): 085017.

Worden K, Farrar CR, Manson G, et al. (2007) The fundamental axioms of structural health monitoring. *Proceedings of the Royal Society A: Mathematical, Physical and Engineering Sciences* 463(2082): 1639–1664.

Yang J, He J, Guan X, et al. (2016) A probabilistic crack size quantification method using in-situ Lamb wave test and Bayesian updating. *Mechanical Systems and Signal Processing* 78: 118–133.

Zhao X, Gao H, Zhang G, et al. (2007) Active health monitoring of an aircraft wing with embedded piezoelectric sensor/actuator network: I. Defect detection, localization and growth monitoring. *Smart Materials and Structures* 16(4): 1208–1217.